

Structural damage detection based on variational Bayesian inference and delayed rejection adaptive Metropolis algorithm

Xiaoyou Wang¹, Rongrong Hou¹, Yong Xia^{1*} and Xiaoqing Zhou²

¹*Department of Civil and Environmental Engineering, The Hong Kong Polytechnic*

University, Kowloon, Hong Kong, China

²*College of Civil Engineering, Shenzhen University, China*

*Corresponding author, email: ceyxia@polyu.edu.hk

Structural damage detection based on variational Bayesian inference and delayed rejection adaptive Metropolis algorithm

ABSTRACT

Existing studies on sparse Bayesian learning for structural damage detection usually assume that the posterior probability density functions (PDFs) follow standard distributions, which facilitates to circumvent the intractable integration problem of the evidence by means of numerical sampling or analytical derivation. Moreover, the uncertainties of each mode are usually quantified as a common parameter to simplify the calculation. These assumptions may not be realistic in practice. This study proposes a sparse Bayesian method for structural damage detection suitable for standard and nonstandard probability distributions. The uncertainty corresponding to each mode is assumed as different. Variational Bayesian inference (VBI) is developed and the posterior PDFs of each unknown is individually derived. The parameters are found to follow the gamma distribution, whereas the distribution of the damage index cannot be directly obtained because of the nonlinear relationship in its posterior PDF. The delayed rejection adaptive Metropolis algorithm is then adopted to generate numerical samples of the damage index. The coupled damage index and parameters in the VBI are successively calculated via an iterative process. A laboratory tested frame is utilised to verify the effectiveness of the proposed method. The results indicate that the sparse damage can be accurately detected. The proposed method has the advantage of high accuracy and broad applicability.

Key words

Damage detection, sparse Bayesian learning, uncertainty, variational Bayesian inference, delayed rejection adaptive Metropolis algorithm

1. Introduction

Vibration-based damage detection contains uncertainties, including measurement noises, methodology errors and modelling errors.¹⁻³ However, Neglect of the uncertainties may lead to inaccurate damage detection results^{4,5} In recent years, several researchers have proposed statistical damage identification approaches using vibration data, where the uncertainties are described as random variables. The representative approaches include perturbation techniques,^{3,6} Monte Carlo simulation,⁷ statistical pattern recognition⁸ and Bayesian methods.⁹⁻¹³ Among these methods, the Bayesian inference provides a rigorous probabilistic framework to identify the target variable and to evaluate the corresponding uncertainties using the available information, and has attracted considerable attention since the 1990s.⁹ Huang et al.¹³ reviewed Bayesian inference in system identification and damage assessment of civil infrastructures.

Given that damage usually occurs at limited positions in the preliminary stage of structural failure, the sparse Bayesian learning,¹⁴ which is widely applied to sparse signal reconstruction and compressed sensing,^{15,16} has been developed for structural damage identification.¹⁷⁻²¹ However, the integral in the evidence of the Bayesian equation for model updating is generally high dimensional and complicated, making the calculation of the posterior probability density function (PDF) difficult. Analytical and numerical techniques have been developed to circumvent this problem.

In regard to the analytical methods, Huang et al.¹⁷ proposed a hierarchical Bayesian model by expanding the nonlinear problem as multiple linear regression functions. This model was improved for damage detection with large modelling errors.¹⁸ However, the hierarchical model introduces extra hyper-parameters that required to be calculated, resulting in a nontrivial workload. Wang et al.²¹ used the Laplace approximation by assuming the nonlinear posterior PDF as Gaussian distribution such that the damage index can be derived in an analytical form. The drawback of the

Laplace approximation is that it only works well when the objective function is globally identified and sharply peaked. In most cases, the condition may not be satisfied because of the limitation of measurement data. In locally identifiable and unidentifiable cases, finding all the optimal modes or eligible points is a computationally challenging and nontrivial task, especially in high-dimensional and nonconvex optimisations.^{23,24}

As for the numerical techniques, the Gibbs sampling was employed by Huang et al.¹⁹ to provide a full Bayesian treatment of the posterior uncertainty. However, Gibbs sampling²² can only be used when the posterior PDF obeys the standard distribution. Hou et al.²⁰ utilised the expectation–maximisation algorithm to calculate the latent damage index via an iterative process. The posterior PDF is assumed to follow a standard Gaussian distribution for sampling in the calculation of expectations. This assumption of the standard Gaussian distribution may not be true in practice.

This study aims to propose an algorithm with wide applicability, high efficiency and accuracy for structural damage detection based on the sparse Bayesian learning. Rather than focusing on the most probable value estimated on the basis of the maximum a posteriori (MAP) principle, this study attempts to provide a full Bayesian treatment by taking the uncertainties of all unknowns into calculation. Therefore, variational Bayesian inference (VBI)²⁵ is developed to derive the posterior PDF of each parameter and variable individually. The mechanism of VBI is to propose a tractable PDF to approximate the target PDF, and through minimizing the Kullback–Leibler (KL) divergence between the proposed and target PDFs, to circumvent the intractable integration in the Bayesian formulation²⁵. Mean field theory²⁶ is utilised to factorise the proposed PDF and independently derive the posterior PDFs of each individual unknown.^{27–29} By employing VBI in this study, the probabilistic expressions proportional to the posterior PDF of each damage index and parameter can be derived. However, the specific distribution of the damage index cannot be directly calculated from the proportional expression because of the nonlinear

relationship between the latent variable and modal parameters. The unidentifiable PDF of the damage index makes its statistical characteristics unavailable and further hinders the iteration progress in the VBI. Therefore, an effective technique should be developed.

Previous studies^{30–32} have indicated that provided that the probabilistic expression proportional to the target PDF is available, the Metropolis–Hastings (MH) algorithm, as a sampling technique developed from the basic Markov chain Monte Carlo (MCMC) simulation, can be utilised to generate samples following the target PDF and obtain the corresponding statistical characteristics no matter how complicated the PDF is. Therefore, the MH algorithm is able to solve the aforementioned unrecognizable problem in the VBI. The basic MH algorithm has been modified to improve its computational efficiency^{33–40} in recent decades. For example, the transitional MCMC is developed for cases when the proposed distribution is difficult to ascertain, and successive intermediate PDFs are used to gradually approach the target PDF.³⁵ The delayed rejection (DR) technique is proposed to improve the acceptance ratio during the sampling process of high-dimensional models.^{38–40} The DR adaptive Metropolis (DRAM) algorithm,⁴¹ as a combination of the adaptive MH algorithm and DR, has been applied in civil engineering.^{42–44} Zhang et al.⁴³ applied this algorithm to a Bayesian model updating and accurately predicted the structural responses. Wan et al.⁴⁴ demonstrated that the DRMA algorithm outperforms the Laplace approximation in model updating when the posterior PDF is a non-normal shape. In this regard, the DRAM algorithm is employed here to generate samples following the posterior PDF which is intractable in the VBI.

In this study, the VBI is combined with the DRAM algorithm for sparse damage detection. The posterior PDFs of the damage index and parameters are individually derived, and all unknowns are then calculated iteratively. A full Bayesian treatment of the posterior uncertainties is conducted during the iteration.

The rest of this paper is organised as follows. The sparse Bayesian framework for structural damage detection based on model updating is introduced and the difficulty in calculating the damage index is explained in Section 2. The VBI is developed to derive the individual posterior PDF of the damage index and each parameter in Section 3, followed by the DRAM algorithm in Section 4. Section 5 summarizes the proposed VBI-DRAM method. The application of the method to an experimental frame is given in Section 6, followed by the conclusions in Section 7.

2. Sparse Bayesian Method for Model Updating

In the Bayesian probabilistic framework, the posterior PDF is derived by updating the likelihood function with the prior information. The likelihood function is founded on the available measurement data, whereas the prior information is empirically determined. The model with regard to the application of the Bayesian theorem to structural model updating is formulated as⁹

$$p(\boldsymbol{\theta}|\mathcal{D}, \mathcal{M}) = p(\mathcal{D}|\boldsymbol{\theta}, \mathcal{M})p(\boldsymbol{\theta}|\mathcal{M})/p(\mathcal{D}|\mathcal{M}) \quad (1)$$

where \mathcal{M} denotes the parameterised model, \mathcal{D} denotes the measurements, $\boldsymbol{\theta}$ is the target variable, $p(\boldsymbol{\theta}|\mathcal{D}, \mathcal{M})$ is the posterior PDF, $p(\mathcal{D}|\boldsymbol{\theta}, \mathcal{M})$ is the likelihood function, $p(\boldsymbol{\theta}|\mathcal{M})$ is the prior PDF, and the denominator $p(\mathcal{D}|\mathcal{M})$ is the normalising constant that is independent of the variable.

2.1 Model class

The model class \mathcal{M} is supposed as a linear model. In the undamaged state, the mass and stiffness matrices in the finite element model (FEM) are formulated as

$$\mathbf{M} = \sum_{i=1}^n \rho_i \mathbf{M}_i \quad (2)$$

$$\mathbf{K} = \sum_{i=1}^n s_i \mathbf{K}_i \quad (3)$$

where \mathbf{M} and \mathbf{K} are the structural global mass and stiffness matrix, respectively, \mathbf{M}_i and \mathbf{K}_i are the elemental mass and stiffness matrix, respectively, ρ_i and s_i are the elemental mass and stiffness parameter, respectively, and n is the number of elements. In the damaged state, suppose that the mass remains unchanged, whereas the stiffness reduces to

$$\bar{\mathbf{K}} = \sum_{i=1}^n \bar{s}_i \mathbf{K}_i \quad (4)$$

where \bar{s}_i is the element stiffness parameter in the damaged state. The stiffness reduction factor (SRF) is defined as⁴⁵

$$\theta_i = \frac{\bar{s}_i - s_i}{s_i} \quad (5)$$

where θ_i is nonpositive and larger than -1 . Consequently, the target variable $\boldsymbol{\theta} = [\theta_1, \theta_2, \dots, \theta_n]$ in Eq. (1) is regarded as the damage index, indicating the damage position and severity of the structure.

2.2 Likelihood PDF

The modal based Bayesian model updating aims to minimise the discrepancy between the measured modal data and model predictions. According to the principle of maximum entropy, the discrepancy is assumed to follow the Gaussian distribution.

The difference between the model predictions and measurements is subjected to measurement noises and modelling errors. The two sources do not exhibit an identical error for each frequency and mode shape. Therefore, the error of each modal parameter is individually evaluated as

$$\boldsymbol{\varepsilon}_r = \frac{\hat{\lambda}_r - \lambda_r(\boldsymbol{\theta})}{\hat{\lambda}_r} \sim \mathcal{N}(0, \beta_r^{-1}) \quad (6)$$

$$\mathbf{e}_r = \hat{\boldsymbol{\phi}}_r - \boldsymbol{\phi}_r(\boldsymbol{\theta}) \sim \mathcal{N}(\mathbf{0}, \gamma_r^{-1} \mathbf{I}) \quad (7)$$

where $\lambda_r(\boldsymbol{\theta})$ and $\boldsymbol{\phi}_r(\boldsymbol{\theta})$ represent the model predicted eigenvalues and mode

shapes, respectively, $\hat{\lambda}_r$ and $\hat{\phi}_r$ are the measured counterparts, and β_r and γ_r reflect the corresponding uncertainty levels.

According to Eqs. (6) and (7), the likelihood functions of the measured frequency and mode shape are formulated as

$$p(\hat{\lambda}_r|\boldsymbol{\theta}, \beta_r) = \left(\frac{\beta_r}{2\pi}\right)^{\frac{1}{2}} \exp\left\{-\frac{1}{2}\beta_r \cdot \left[\frac{\hat{\lambda}_r - \lambda_r(\boldsymbol{\theta})}{\hat{\lambda}_r}\right]^2\right\} \quad (8)$$

$$p(\hat{\phi}_r|\boldsymbol{\theta}, \gamma_r) = \left(\frac{\gamma_r}{2\pi}\right)^{\frac{N_p}{2}} \exp\left\{-\frac{1}{2}\gamma_r \cdot \|\hat{\phi}_r - \phi_r(\boldsymbol{\theta})\|_2^2\right\} \quad (9)$$

The modal parameters are assumed to be independent from mode to mode. Therefore, the resulting likelihood functions of $\boldsymbol{\theta}$ based on measured modal parameters $\hat{\boldsymbol{\lambda}}$ and $\hat{\boldsymbol{\psi}}$ are expressed as

$$p(\hat{\boldsymbol{\lambda}}|\boldsymbol{\theta}, \boldsymbol{\beta}) = \prod_{r=1}^{N_m} p(\hat{\lambda}_r|\boldsymbol{\theta}, \beta_r) = \left(\prod_{r=1}^{N_m} \frac{\beta_r}{2\pi}\right)^{\frac{1}{2}} \exp\left\{-\frac{1}{2}\sum_{r=1}^{N_m} \left(\beta_r \cdot \left[\frac{\hat{\lambda}_r - \lambda_r(\boldsymbol{\theta})}{\hat{\lambda}_r}\right]^2\right)\right\} \quad (10)$$

$$p(\hat{\boldsymbol{\psi}}|\boldsymbol{\theta}, \boldsymbol{\gamma}) = \prod_{r=1}^{N_m} p(\hat{\phi}_r|\boldsymbol{\theta}, \gamma_r) = \left(\prod_{r=1}^{N_m} \frac{\gamma_r}{2\pi}\right)^{\frac{N_p}{2}} \exp\left\{-\frac{1}{2}\sum_{r=1}^{N_m} (\gamma_r \cdot \|\hat{\phi}_r - \phi_r(\boldsymbol{\theta})\|_2^2)\right\} \quad (11)$$

where N_m is the number of measured modes.

2.3 Prior PDF

The identification of the SRF is a typical ill-posed inverse problem.⁴⁶ To solve this problem, the regularisation techniques, such as l_1 and l_2 techniques,⁴⁵⁻⁴⁸ have been applied to structural model updating given that damage usually occur at limited locations in the preliminary stage of the structural failure. In the Bayesian framework, it is suggested to adopt the conjugate prior to simplify the calculation. However, the l_1 technique is not conjugated to the Gaussian distribution adopted in the likelihood function. Tippling¹⁴ proposed the sparse Bayesian learning, where the prior is formulated based on the automatic relevance determination (ARD) principle. The

ARD model following the Gaussian distribution is conjugated to the likelihood function in this study and adopted as the prior, which is expressed as

$$p(\boldsymbol{\theta}|\boldsymbol{\alpha}) = \prod_{i=1}^n p(\theta_i|\alpha_i) = \left(\frac{1}{2\pi}\right)^{\frac{n}{2}} \prod_{i=1}^n \left[\alpha_i^{\frac{1}{2}} \exp\left\{-\frac{1}{2}\alpha_i\theta_i^2\right\} \right] \quad (12)$$

where α_i represents the precision of θ_i .

2.4 Posterior PDF

Substituting Eqs. (10)–(12) into Eq. (1), the posterior PDF of the damage index is formulated as

$$\begin{aligned} p(\boldsymbol{\theta}|\hat{\boldsymbol{\lambda}}, \hat{\boldsymbol{\Psi}}, \boldsymbol{\alpha}, \boldsymbol{\beta}, \boldsymbol{\gamma}) &= \frac{p(\hat{\boldsymbol{\lambda}}, \hat{\boldsymbol{\Psi}}|\boldsymbol{\theta}, \boldsymbol{\beta}, \boldsymbol{\gamma})p(\boldsymbol{\theta}|\boldsymbol{\alpha})}{p(\hat{\boldsymbol{\lambda}}, \hat{\boldsymbol{\Psi}}|\boldsymbol{\alpha}, \boldsymbol{\beta}, \boldsymbol{\gamma})} = \frac{p(\hat{\boldsymbol{\lambda}}|\boldsymbol{\theta}, \boldsymbol{\beta})p(\hat{\boldsymbol{\Psi}}|\boldsymbol{\theta}, \boldsymbol{\gamma})p(\boldsymbol{\theta}|\boldsymbol{\alpha})}{\int p(\hat{\boldsymbol{\lambda}}, \hat{\boldsymbol{\Psi}}, \boldsymbol{\theta}|\boldsymbol{\alpha}, \boldsymbol{\beta}, \boldsymbol{\gamma})d\boldsymbol{\theta}} \\ &= c^{-1} p(\hat{\boldsymbol{\lambda}}|\boldsymbol{\theta}, \boldsymbol{\beta})p(\hat{\boldsymbol{\Psi}}|\boldsymbol{\theta}, \boldsymbol{\gamma})p(\boldsymbol{\theta}|\boldsymbol{\alpha}) \\ &= c^{-1} \left(\prod_{r=1}^{N_m} \frac{\beta_r}{2\pi} \right)^{\frac{1}{2}} \left(\prod_{r=1}^{N_m} \frac{\gamma_r}{2\pi} \right)^{\frac{N_p}{2}} \left(\frac{1}{2\pi} \right)^{\frac{n}{2}} \left(\prod_{i=1}^n \alpha_i^{\frac{1}{2}} \right) \exp \left\{ -\frac{1}{2} \sum_{r=1}^{N_m} \left(\beta_r \cdot \left[\frac{\hat{\lambda}_r - \lambda_r(\boldsymbol{\theta})}{\hat{\lambda}_r} \right]^2 \right) \right. \\ &\quad \left. - \frac{1}{2} \sum_{r=1}^{N_m} \left(\gamma_r \cdot \|\hat{\boldsymbol{\phi}}_r - \boldsymbol{\phi}_r(\boldsymbol{\theta})\|_2^2 \right) - \frac{1}{2} \sum_{i=1}^n (\alpha_i \theta_i^2) \right\} \end{aligned} \quad (13)$$

where the evidence $c = \int p(\hat{\boldsymbol{\lambda}}, \hat{\boldsymbol{\Psi}}, \boldsymbol{\theta}|\boldsymbol{\alpha}, \boldsymbol{\beta}, \boldsymbol{\gamma})d\boldsymbol{\theta}$ is calculated by marginalising damage index $\boldsymbol{\theta}$ and is therefore independent of $\boldsymbol{\theta}$.

The MAP estimation to the damage index in Eq. (13) is equivalent to minimising the negative natural logarithm of the posterior PDF, which is written as

$$\begin{aligned} \bar{\boldsymbol{\theta}} &= \arg \min J(\boldsymbol{\theta}) \\ &= \arg \min \sum_{r=1}^{N_m} \left(\beta_r \left[\frac{\hat{\lambda}_r - \lambda_r(\boldsymbol{\theta})}{\hat{\lambda}_r} \right]^2 \right) + \sum_{r=1}^{N_m} \left(\gamma_r \|\hat{\boldsymbol{\phi}}_r - \boldsymbol{\phi}_r(\boldsymbol{\theta})\|_2^2 \right) + \sum_{i=1}^n (\alpha_i \theta_i^2) \end{aligned} \quad (14)$$

The items unrelated with $\boldsymbol{\theta}$ are omitted in the above equation. The minimisation of Eq. (14) cannot be directly obtained because parameters $\{\boldsymbol{\alpha}, \boldsymbol{\beta}, \boldsymbol{\gamma}\}$ are unknown. VBI is used to solve this problem in the subsequent section.

3. VBI

The mechanism of VBI is to propose a tractable PDF to approximate the target PDF.²⁵ In this study, the target PDF is the posterior PDF $p(\boldsymbol{\theta}|\hat{\boldsymbol{\lambda}}, \hat{\boldsymbol{\Psi}}, \boldsymbol{\alpha}, \boldsymbol{\beta}, \boldsymbol{\gamma})$, and the proposed PDF is symbolised as $\boldsymbol{Q}(\boldsymbol{\theta}, \boldsymbol{\alpha}, \boldsymbol{\beta}, \boldsymbol{\gamma})$, which is simplified as \boldsymbol{Q} .

According to Eq. (13), the evidence can be calculated as

$$c = p(\hat{\boldsymbol{\lambda}}, \hat{\boldsymbol{\Psi}}|\boldsymbol{\alpha}, \boldsymbol{\beta}, \boldsymbol{\gamma}) = \frac{p(\hat{\boldsymbol{\lambda}}|\boldsymbol{\theta}, \boldsymbol{\beta})p(\hat{\boldsymbol{\Psi}}|\boldsymbol{\theta}, \boldsymbol{\gamma})p(\boldsymbol{\theta}|\boldsymbol{\alpha})}{p(\boldsymbol{\theta}|\hat{\boldsymbol{\lambda}}, \hat{\boldsymbol{\Psi}}, \boldsymbol{\alpha}, \boldsymbol{\beta}, \boldsymbol{\gamma})} = \frac{p(\hat{\boldsymbol{\lambda}}, \hat{\boldsymbol{\Psi}}, \boldsymbol{\theta}|\boldsymbol{\alpha}, \boldsymbol{\beta}, \boldsymbol{\gamma})}{p(\boldsymbol{\theta}|\hat{\boldsymbol{\lambda}}, \hat{\boldsymbol{\Psi}}, \boldsymbol{\alpha}, \boldsymbol{\beta}, \boldsymbol{\gamma})} \quad (15)$$

Taking the logarithm of the two sides in Eq. (15), the formulation changes into

$$\begin{aligned} \ln p(\hat{\boldsymbol{\lambda}}, \hat{\boldsymbol{\Psi}}|\boldsymbol{\alpha}, \boldsymbol{\beta}, \boldsymbol{\gamma}) &= \ln \frac{p(\hat{\boldsymbol{\lambda}}, \hat{\boldsymbol{\Psi}}, \boldsymbol{\theta}|\boldsymbol{\alpha}, \boldsymbol{\beta}, \boldsymbol{\gamma})}{p(\boldsymbol{\theta}|\hat{\boldsymbol{\lambda}}, \hat{\boldsymbol{\Psi}}, \boldsymbol{\alpha}, \boldsymbol{\beta}, \boldsymbol{\gamma})} \\ &= \ln \frac{p(\hat{\boldsymbol{\lambda}}, \hat{\boldsymbol{\Psi}}, \boldsymbol{\theta}|\boldsymbol{\alpha}, \boldsymbol{\beta}, \boldsymbol{\gamma})}{\boldsymbol{Q}} - \ln \frac{p(\boldsymbol{\theta}|\hat{\boldsymbol{\lambda}}, \hat{\boldsymbol{\Psi}}, \boldsymbol{\alpha}, \boldsymbol{\beta}, \boldsymbol{\gamma})}{\boldsymbol{Q}} \end{aligned} \quad (16)$$

where \boldsymbol{Q} is the proposed PDF to approximate $p(\boldsymbol{\theta}|\hat{\boldsymbol{\lambda}}, \hat{\boldsymbol{\Psi}}, \boldsymbol{\alpha}, \boldsymbol{\beta}, \boldsymbol{\gamma})$. Taking the expectation of the two sides in Eq. (16) with respect to \boldsymbol{Q} yields

$$\begin{aligned} &\int \boldsymbol{Q} \ln p(\hat{\boldsymbol{\lambda}}, \hat{\boldsymbol{\Psi}}|\boldsymbol{\alpha}, \boldsymbol{\beta}, \boldsymbol{\gamma}) d\boldsymbol{\theta} \\ &= \int \boldsymbol{Q} \ln \frac{p(\hat{\boldsymbol{\lambda}}, \hat{\boldsymbol{\Psi}}, \boldsymbol{\theta}|\boldsymbol{\alpha}, \boldsymbol{\beta}, \boldsymbol{\gamma})}{\boldsymbol{Q}} d\boldsymbol{\theta} - \int \boldsymbol{Q} \ln \frac{p(\boldsymbol{\theta}|\hat{\boldsymbol{\lambda}}, \hat{\boldsymbol{\Psi}}, \boldsymbol{\alpha}, \boldsymbol{\beta}, \boldsymbol{\gamma})}{\boldsymbol{Q}} d\boldsymbol{\theta} \end{aligned} \quad (17)$$

Given that $\ln p(\hat{\boldsymbol{\lambda}}, \hat{\boldsymbol{\Psi}}|\boldsymbol{\alpha}, \boldsymbol{\beta}, \boldsymbol{\gamma})$ is irrelevant to $\boldsymbol{\theta}$, the left side of Eq. (17) is equivalent to $\ln p(\hat{\boldsymbol{\lambda}}, \hat{\boldsymbol{\Psi}}|\boldsymbol{\alpha}, \boldsymbol{\beta}, \boldsymbol{\gamma})$. Therefore, Eq. (17) can be simplified as

$$\ln p(\hat{\boldsymbol{\lambda}}, \hat{\boldsymbol{\Psi}}|\boldsymbol{\alpha}, \boldsymbol{\beta}, \boldsymbol{\gamma}) = \mathcal{L}(\boldsymbol{Q}) + D_{KL}\{\boldsymbol{Q}||p(\boldsymbol{\theta}|\hat{\boldsymbol{\lambda}}, \hat{\boldsymbol{\Psi}}, \boldsymbol{\alpha}, \boldsymbol{\beta}, \boldsymbol{\gamma})\} \quad (18)$$

where

$$\mathcal{L}(\boldsymbol{Q}) = E_{\boldsymbol{Q}} \left[\ln \frac{p(\hat{\boldsymbol{\lambda}}, \hat{\boldsymbol{\Psi}}, \boldsymbol{\theta}|\boldsymbol{\alpha}, \boldsymbol{\beta}, \boldsymbol{\gamma})}{\boldsymbol{Q}} \right] \quad (19)$$

$$D_{KL}\{\mathbf{Q}||p(\boldsymbol{\theta}|\hat{\boldsymbol{\lambda}}, \hat{\boldsymbol{\Psi}}, \boldsymbol{\alpha}, \boldsymbol{\beta}, \boldsymbol{\gamma})\} = \int \mathbf{Q} \ln \frac{\mathbf{Q}}{p(\boldsymbol{\theta}|\hat{\boldsymbol{\lambda}}, \hat{\boldsymbol{\Psi}}, \boldsymbol{\alpha}, \boldsymbol{\beta}, \boldsymbol{\gamma})} d\boldsymbol{\theta} \quad (20)$$

where $E_{\mathbf{Q}}$ denotes the expectation with respect to \mathbf{Q} , $\mathcal{L}(\mathbf{Q})$ represents the lower bound of \mathbf{Q} and D_{KL} is the KL divergence²⁵ between \mathbf{Q} and posterior PDF $p(\boldsymbol{\theta}|\hat{\boldsymbol{\lambda}}, \hat{\boldsymbol{\Psi}}, \boldsymbol{\alpha}, \boldsymbol{\beta}, \boldsymbol{\gamma})$.

It has been proved that $D_{KL} \geq 0$.²⁵ $D_{KL} = 0$ when $\mathbf{Q} = p(\boldsymbol{\theta}|\hat{\boldsymbol{\lambda}}, \hat{\boldsymbol{\Psi}}, \boldsymbol{\alpha}, \boldsymbol{\beta}, \boldsymbol{\gamma})$. Therefore, increasing the proximity of \mathbf{Q} to the posterior PDF is equivalent to minimising D_{KL} . As the posterior PDF $p(\boldsymbol{\theta}|\hat{\boldsymbol{\lambda}}, \hat{\boldsymbol{\Psi}}, \boldsymbol{\alpha}, \boldsymbol{\beta}, \boldsymbol{\gamma})$ is unknown, D_{KL} cannot be calculated directly. According to Eq.(18), minimising D_{KL} is equivalent to maximise $\mathcal{L}(\mathbf{Q})$.²⁵ To obtain the independent posterior PDF of the damage index and parameters, \mathbf{Q} is factorized into two components based on the mean field theory,²⁶ shown as

$$\mathbf{Q}(\boldsymbol{\theta}, \boldsymbol{\alpha}, \boldsymbol{\beta}, \boldsymbol{\gamma}) = q(\boldsymbol{\theta})q(\boldsymbol{\alpha}, \boldsymbol{\beta}, \boldsymbol{\gamma}) \quad (21)$$

The maximisation of $\mathcal{L}(\mathbf{Q})$ can be achieved by optimising each factor in turn through solving the expectation of the numerator $p(\hat{\boldsymbol{\lambda}}, \hat{\boldsymbol{\Psi}}, \boldsymbol{\theta}|\boldsymbol{\alpha}, \boldsymbol{\beta}, \boldsymbol{\gamma})$ in $\mathcal{L}(\mathbf{Q})$ with respect to other factors.²⁵ Therefore, factor $q(\boldsymbol{\alpha}, \boldsymbol{\beta}, \boldsymbol{\gamma})$ can be derived by calculating the expectation of $\ln p(\hat{\boldsymbol{\lambda}}, \hat{\boldsymbol{\Psi}}, \boldsymbol{\theta}|\boldsymbol{\alpha}, \boldsymbol{\beta}, \boldsymbol{\gamma})$ with respect to $\boldsymbol{\theta}$, that is

$$\begin{aligned} \ln q(\boldsymbol{\alpha}, \boldsymbol{\beta}, \boldsymbol{\gamma}) &= E_{\boldsymbol{\theta}}[\ln p(\hat{\boldsymbol{\lambda}}, \hat{\boldsymbol{\Psi}}, \boldsymbol{\theta}|\boldsymbol{\alpha}, \boldsymbol{\beta}, \boldsymbol{\gamma})] + \text{const} \\ &= E_{\boldsymbol{\theta}}[\ln p(\hat{\boldsymbol{\lambda}}|\boldsymbol{\theta}, \boldsymbol{\beta}) + \ln p(\hat{\boldsymbol{\Psi}}|\boldsymbol{\theta}, \boldsymbol{\gamma}) + \ln p(\boldsymbol{\theta}|\boldsymbol{\alpha})] + \text{const} \\ &= \frac{1}{2} \sum_{r=1}^{N_m} \ln \beta_r - \frac{1}{2} \sum_{r=1}^{N_m} \left\{ \beta_r \cdot E_{\boldsymbol{\theta}} \left(\left[\frac{\hat{\lambda}_r - \lambda_r(\boldsymbol{\theta})}{\hat{\lambda}_r} \right]^2 \right) \right\} + \frac{N_p}{2} \sum_{r=1}^{N_m} \ln \gamma_r \\ &\quad - \frac{1}{2} \sum_{r=1}^{N_m} \left\{ \gamma_r \cdot E_{\boldsymbol{\theta}} \left(\|\hat{\boldsymbol{\phi}}_r - \boldsymbol{\phi}_r(\boldsymbol{\theta})\|^2 \right) \right\} + \frac{1}{2} \sum_{i=1}^n \ln \alpha_i - \frac{1}{2} \sum_{i=1}^n \{ \alpha_i E(\theta_i^2) \} + \text{const} \end{aligned} \quad (22)$$

Parameters $\{\boldsymbol{\alpha}, \boldsymbol{\beta}, \boldsymbol{\gamma}\}$ are assumed to be independent from each other and from mode to mode, leading to the factorisation as

$$q(\boldsymbol{\alpha}, \boldsymbol{\beta}, \boldsymbol{\gamma}) = q(\boldsymbol{\alpha})q(\boldsymbol{\beta})q(\boldsymbol{\gamma}) \quad (23)$$

$$q(\boldsymbol{\alpha}) = \prod_{i=1}^n q(\alpha_i) \quad (24)$$

$$q(\boldsymbol{\beta}) = \prod_{r=1}^{N_m} q(\beta_r) \quad (25)$$

$$q(\boldsymbol{\gamma}) = \prod_{r=1}^{N_m} q(\gamma_r) \quad (26)$$

Therefore,

$$\ln q(\boldsymbol{\alpha}, \boldsymbol{\beta}, \boldsymbol{\gamma}) = \sum_{i=1}^n \ln q(\alpha_i) + \sum_{r=1}^{N_m} \ln q(\beta_r) + \sum_{r=1}^{N_m} \ln q(\gamma_r) \quad (27)$$

According to Eq. (22), the logarithm of the posterior PDF of the individual parameter is then obtained as

$$\ln q(\alpha_i) = \frac{1}{2} \ln \alpha_i - \frac{1}{2} \alpha_i E(\theta_i^2) + \text{const} \quad (28)$$

$$\ln q(\beta_r) = \frac{1}{2} \ln \beta_r - \frac{\beta_r}{2} E_{\theta} \left(\left[\frac{\hat{\lambda}_r - \lambda_r(\boldsymbol{\theta})}{\hat{\lambda}_r} \right]^2 \right) + \text{const} \quad (29)$$

$$\ln q(\gamma_r) = \frac{N_p}{2} \ln \gamma_r - \frac{\gamma_r}{2} E_{\theta} \left(\|\hat{\boldsymbol{\phi}}_r - \boldsymbol{\phi}_r(\boldsymbol{\theta})\|_2^2 \right) + \text{const} \quad (30)$$

It shows that all parameters follow the gamma distribution as

$$q(\alpha_i) \propto (\alpha_i)^{\frac{1}{2}} \cdot \exp \left\{ -\frac{\alpha_i}{2} \cdot E(\theta_i^2) \right\} \quad (31)$$

$$q(\beta_r) \propto (\beta_r)^{\frac{1}{2}} \cdot \exp \left\{ -\frac{\beta_r}{2} \cdot E_{\theta} \left(\left[\frac{\hat{\lambda}_r - \lambda_r(\boldsymbol{\theta})}{\hat{\lambda}_r} \right]^2 \right) \right\} \quad (32)$$

$$q(\gamma_r) \propto (\gamma_r)^{\frac{N_p}{2}} \cdot \exp \left\{ -\frac{\gamma_r}{2} \cdot E_{\theta} \left(\|\hat{\boldsymbol{\phi}}_r - \boldsymbol{\phi}_r(\boldsymbol{\theta})\|_2^2 \right) \right\} \quad (33)$$

Therefore, the mean and variance of each parameter are calculated as

$$E(\alpha_i) = \frac{3}{E(\theta_i^2)}; \text{Var}(\alpha_i) = \frac{6}{[E(\theta_i^2)]^2} \quad (34)$$

$$E(\beta_r) = \frac{3}{E_{\theta} \left(\left[\frac{\hat{\lambda}_r - \lambda_r(\boldsymbol{\theta})}{\hat{\lambda}_r} \right]^2 \right)} ; \text{Var}(\beta_r) = \frac{6}{\left\{ E_{\theta} \left(\left[\frac{\hat{\lambda}_r - \lambda_r(\boldsymbol{\theta})}{\hat{\lambda}_r} \right]^2 \right) \right\}^2} \quad (35)$$

$$E(\gamma_r) = \frac{N_p + 2}{E_{\theta} \left(\|\hat{\boldsymbol{\phi}}_r - \boldsymbol{\phi}_r(\boldsymbol{\theta})\|_2^2 \right)} ; \text{Var}(\gamma_r) = \frac{2N_p + 4}{\left[E_{\theta} \left(\|\hat{\boldsymbol{\phi}}_r - \boldsymbol{\phi}_r(\boldsymbol{\theta})\|_2^2 \right) \right]^2} \quad (36)$$

Factor $q(\boldsymbol{\theta})$ can be similarly derived by calculating the expectation of $\ln p(\hat{\boldsymbol{\lambda}}, \hat{\boldsymbol{\psi}}, \boldsymbol{\theta} | \boldsymbol{\alpha}, \boldsymbol{\beta}, \boldsymbol{\gamma})$ with respect to $\{\boldsymbol{\alpha}, \boldsymbol{\beta}, \boldsymbol{\gamma}\}$, that is

$$\begin{aligned} \ln q(\boldsymbol{\theta}) &= E_{\boldsymbol{\alpha}, \boldsymbol{\beta}, \boldsymbol{\gamma}} [\ln p(\hat{\boldsymbol{\lambda}}, \hat{\boldsymbol{\psi}}, \boldsymbol{\theta} | \boldsymbol{\alpha}, \boldsymbol{\beta}, \boldsymbol{\gamma})] + \text{const} \\ &= E_{\boldsymbol{\alpha}, \boldsymbol{\beta}, \boldsymbol{\gamma}} [\ln p(\hat{\boldsymbol{\lambda}} | \boldsymbol{\theta}, \boldsymbol{\beta}) p(\hat{\boldsymbol{\psi}} | \boldsymbol{\theta}, \boldsymbol{\gamma}) p(\boldsymbol{\theta} | \boldsymbol{\alpha})] + \text{const} \\ &= E_{\boldsymbol{\beta}} [\ln p(\hat{\boldsymbol{\lambda}} | \boldsymbol{\theta}, \boldsymbol{\beta})] + E_{\boldsymbol{\gamma}} [\ln p(\hat{\boldsymbol{\psi}} | \boldsymbol{\theta}, \boldsymbol{\gamma})] + E_{\boldsymbol{\alpha}} [p(\boldsymbol{\theta} | \boldsymbol{\alpha})] + \text{const} \\ &= -\frac{1}{2} \sum_{r=1}^{N_m} \left\{ E(\beta_r) \cdot \left[\frac{\hat{\lambda}_r - \lambda_r(\boldsymbol{\theta})}{\hat{\lambda}_r} \right]^2 \right\} - \frac{1}{2} \sum_{r=1}^{N_m} \left\{ E(\gamma_r) \cdot \|\hat{\boldsymbol{\phi}}_r - \boldsymbol{\phi}_r(\boldsymbol{\theta})\|_2^2 \right\} \\ &\quad - \frac{1}{2} \sum_{i=1}^n \{ E(\alpha_i) \cdot \theta_i^2 \} + \text{const} \end{aligned} \quad (37)$$

where the items independent with $\boldsymbol{\theta}$ are merged into the constant item. Therefore,

$$\begin{aligned} q(\boldsymbol{\theta}) \propto \exp \left\{ - \sum_{r=1}^{N_m} \left[\frac{E(\beta_r)}{2} \cdot \left(\frac{\hat{\lambda}_r - \lambda_r(\boldsymbol{\theta})}{\hat{\lambda}_r} \right)^2 \right] \right. \\ \left. - \sum_{r=1}^{N_m} \left[\frac{E(\gamma_r)}{2} \cdot \|\hat{\boldsymbol{\phi}}_r - \boldsymbol{\phi}_r(\boldsymbol{\theta})\|_2^2 \right] - \sum_{i=1}^n \left[\frac{E(\alpha_i)}{2} \cdot \theta_i^2 \right] \right\} \end{aligned} \quad (38)$$

Eqs. (34)–(36) and (38) are coupled and should be iteratively calculated. The iterations are corresponding to the variational Bayesian expectation and maximisation step.²⁵ Given that VBI does not guarantee to converge to the global optimum, it is suggested to assign different initialisations to the parameters at the beginning of the iteration. The iterative process requires the calculation of three expectations, namely, $E(\theta_i^2)$, $E_{\theta} \left(\left[\frac{\hat{\lambda}_r - \lambda_r(\boldsymbol{\theta})}{\hat{\lambda}_r} \right]^2 \right)$ and $E_{\theta} \left(\|\hat{\boldsymbol{\phi}}_r - \boldsymbol{\phi}_r(\boldsymbol{\theta})\|_2^2 \right)$, which is a full Bayesian analysis that takes posterior uncertainties of $\boldsymbol{\theta}$ into consideration. However, the specific distribution of $\boldsymbol{\theta}$ cannot be directly recognised from Eq. (38) because of the

nonlinear relationship between θ and the modal parameters. This scenario hinders the iteration progress in the VBI. In next section the numerical DRAM algorithm is used to obtain the statistical distribution of θ .

4. DRAM Algorithm

The MH algorithm is one of the most common MCMC simulation and can be used to generate samples following the target PDF that is difficult to directly sample [31]. Given the expression $q(y)$ proportional to the target PDF and proposed PDF S to generate samples, the procedures of the basic MH algorithm are described as follows:³¹

- (1) Generate the candidate sample $y \sim S(\cdot | x^j)$, where x^j is the current sample,
- (2) Compute the acceptance ratio of the candidate sample,

$$\xi(x^j, y) = \min \left\{ 1, \frac{q(y)S(y|x^j)}{q(x^j)S(x^j|y)} \right\}$$

- (3) The next sample is

$$x^{j+1} = \begin{cases} y & \text{with the acceptance ratio } \xi(x^j, y) \\ x^j & \text{with the rejection ratio } 1 - \xi(x^j, y) \end{cases}$$

The sample will eventually converge to its equilibrium distribution after the burn-in period.³⁰ However, the rejection ratio of samples in high-dimensional problems is usually large because of the wide sampling space. Accordingly, the burn-in period will be long, resulting in a low sampling efficiency. To solve this problem, DR^{39,40} algorithm is proposed to reduce the number of rejected samples and improve the acceptance ratio. When the candidate sample is decided to be rejected, rather than getting a repeated sample, a secondary candidate sample is generated from an adjusted proposal PDF and the acceptance ratio is recalculated. This process is called DR and the procedures are as follow:^{39, 40}

- (1) Generate the candidate sample $y_1 \sim S(\cdot | x^j)$, where x^j is the current sample,

(2) Compute the acceptance ratio of the candidate sample,

$$\xi_1(x^j, y_1) = \min \left\{ 1, \frac{q(y_1)S(y_1|x^j)}{q(x^j)S(x^j|y_1)} \right\}$$

(3) The next sample is

$$x^{j+1} = \begin{cases} y_1 \text{ and go to Step (7)} & \text{with the acceptance ratio } \xi_1(x^j, y_1) \\ \text{go to Step (4)} & \text{with the rejection ratio } 1 - \xi_1(x^j, y_1) \end{cases}$$

(4) Generate the candidate sample $y_2 \sim S(\cdot | x^j, y_1)$,

(5) Compute the acceptance ratio of the secondary candidate sample,

$$\xi_2(x^j, y_1, y_2) = \min \left\{ 1, \frac{q(y_2)S(y_1|y_2)S(x^j|y_1, y_2)(1 - \xi_1(y_2, y_1))}{q(x^j)S(y_1|x^j)S(y_2|x^j, y_1)(1 - \xi_1(x^j, y_1))} \right\}$$

(6) The next sample is

$$x^{j+1} = \begin{cases} y_2 & \text{with the acceptance ratio } \xi_2(x^j, y_1, y_2) \\ x^j & \text{with rejection ratio } \xi_2(x^j, y_1, y_2) \end{cases}$$

(7) End

Moreover, the proposed PDF for sampling also significantly influences the sampling efficiency.^{30,31} The closer the proposed PDF is to the target PDF, the higher the acceptance ratio of the sample will be. In most instances, the Gaussian distribution is adopted as the proposed PDF because of its operability and large entropy. The mean of Gaussian distribution is consistently adjusted with the new obtained sample as shown above, whereas the variance is generally determined based on experience. A small variance results in a slow convergence when the sample severely deviates from the equilibrium distribution, whereas a large variance leads to a high sampling rejection ratio. In light of this issue, the adaptive Metropolis (AM) algorithm^{36,37} is proposed to automatically adjust the variance based on the generated samples. The adjustment is usually conducted after obtaining a certain number of samples to ensure the semi-positive definite property of the covariance matrix. The adjustment rule is expressed as^{36,37}

$$C = \begin{cases} C, j + 1 < N_t \\ S_d \text{cov}(\boldsymbol{\theta}^{(1)}, \boldsymbol{\theta}^{(2)}, \dots, \boldsymbol{\theta}^{(j+1)}) + S_d \varepsilon \mathbf{I}_d, j + 1 \geq N_t \end{cases} \quad (39)$$

where C is the covariance matrix which is usually determined based on experience, S_d is a parameter related to the dimension of the covariance and is generally set to $2.4^2/d$ (d is the dimension of $\boldsymbol{\theta}$),⁴¹ ε is an extremely minimal constant, \mathbf{I}_d is an identity matrix, and N_t is the bound number of samples before the adjustment of the covariance matrix.

Considering the advantages of DR and AM algorithms, researchers have combined them to generate a new algorithm called the DRAM algorithm.⁴¹ The DRAM algorithm is applicable to standard and nonstandard probabilistic distributions, provided that the probability proportional to the target PDF is available. It has a considerable efficiency when applied to high-dimensional problems.⁴⁴

In this study, the DRAM algorithm is used to generate samples of $\boldsymbol{\theta}$ using Eq. (38). For simplification and efficiency, a two-layer delayed rejection is employed. That is, if the secondary sample is rejected, the new sample is set equal the previous sample and the third-layer sampling is not performed any more. A Gaussian distribution $\mathcal{N}(\mu, C)$ is adopted as the proposed PDF. To accelerate the convergence and shorten the burn-in period of the DRAM algorithm, the mean μ of the Gaussian distribution is initially set as $\bar{\boldsymbol{\theta}}$, which is calculated from the minimisation of the objective function in Eq. (14). Both the mean μ and covariance matrix C are adjusted with the progress of sampling. The algorithm is described as follows:

DRAM algorithm

Given the proposed sampling PDF $\mathcal{N}(\mu, C)$, the first sample $\boldsymbol{\theta}^{(1)}$, the scale factor ρ to reduce the covariance ($\rho < 1$), the bound N_t , the trivial constant ε and the number of samples n_s

1. Generate the candidate sample $x_1 \sim \mathcal{N}(\mu, C)$.
-

2. Calculate the acceptance ratio of the candidate sample,

$$\xi_{j1}(\boldsymbol{\theta}^{(j)}, x_1) = \min \left\{ 1, \frac{q(x_1)\mathcal{N}_{\boldsymbol{\theta}^{(j)}}(x_1, C)}{q(\boldsymbol{\theta}^{(j)})\mathcal{N}_{x_1}(\boldsymbol{\theta}^{(j)}, C)} \right\}$$

3. Randomly generate $\boldsymbol{\mu}$ from uniform distribution $\mathcal{U}(0, 1)$.

4. If $\boldsymbol{\mu} < \xi_{j1}(\boldsymbol{\theta}^{(j)}, x_1)$, $\boldsymbol{\theta}^{(j+1)} = x_1$, and go to Step 8. Otherwise, go to Step 5.

5. Generate the secondary candidate sample $x_2 \sim \mathcal{N}(\boldsymbol{\mu}, \rho C)$.

6. Calculate the acceptance ratio of the secondary candidate sample,

$$\xi_{j2}(x_2, x_1) = \min \left\{ 1, \frac{q(x_2)\mathcal{N}_{x_2}(x_1, C_0)}{q(x_1)\mathcal{N}_{x_1}(x_2, C_0)} \right\}$$

$$\xi_{j2}(\boldsymbol{\theta}^{(j)}, x_2) = \min \left\{ 1, \frac{q(x_2)\mathcal{N}_{x_1}(x_2, C)\mathcal{N}_{\boldsymbol{\theta}^{(j)}}(x_2, C)[1 - \xi_{j2}(x_2, x_1)]}{q(\boldsymbol{\theta}^{(j)})\mathcal{N}_{x_1}(\boldsymbol{\theta}^{(j)}, C)\mathcal{N}_{x_2}(\boldsymbol{\theta}^{(j)}, C)[1 - \xi_{j1}(\boldsymbol{\theta}^{(j)}, x_1)]} \right\}$$

7. If $\boldsymbol{\mu} < \xi_{j2}(\boldsymbol{\theta}^{(j)}, x_2)$, then $\boldsymbol{\theta}^{(j+1)} = x_2$. Else, $\boldsymbol{\theta}^{(j+1)} = \boldsymbol{\theta}^{(j)}$.

8. Adjust the sampling covariance

$$C = \begin{cases} C, & j + 1 < N_t \\ S_d \text{cov}(\boldsymbol{\theta}^{(1)}, \boldsymbol{\theta}^{(2)}, \dots, \boldsymbol{\theta}^{(j+1)}) + S_d \boldsymbol{\varepsilon} \boldsymbol{I}_d, & j + 1 > N_t \end{cases}$$

9. Let $\boldsymbol{\mu} = \boldsymbol{\theta}^{(j+1)}$.

10. Let $j = j + 1$, repeat Steps 1–8 until $j = (n_s - 1)$.

11. The samples following the posterior PDF of $\boldsymbol{\theta}$ is obtained, $(\boldsymbol{\theta}^{(1)}, \boldsymbol{\theta}^{(2)}, \dots, \boldsymbol{\theta}^{(n_s)})$. The most probable value and uncertainty of $\boldsymbol{\theta}$ are calculated from the samples.

5. Summary of the Proposed Method

Figure 1 summarises the implementation procedures of the proposed method, which starts from initialising the parameters and progresses by iteratively updating all unknowns. The damage index $\boldsymbol{\theta}$ are sampled using the DRAM sampling technique according to Eqs. (14) and (38), and the most probable value $\boldsymbol{\theta}_{\text{MAP}}$ is calculated from the obtained samples. The parameters $\{\boldsymbol{\alpha}, \boldsymbol{\beta}, \boldsymbol{\gamma}\}$ are updated according to Eqs. (34)–(36). The procedures are repeated until the defined convergence criterion is satisfied.

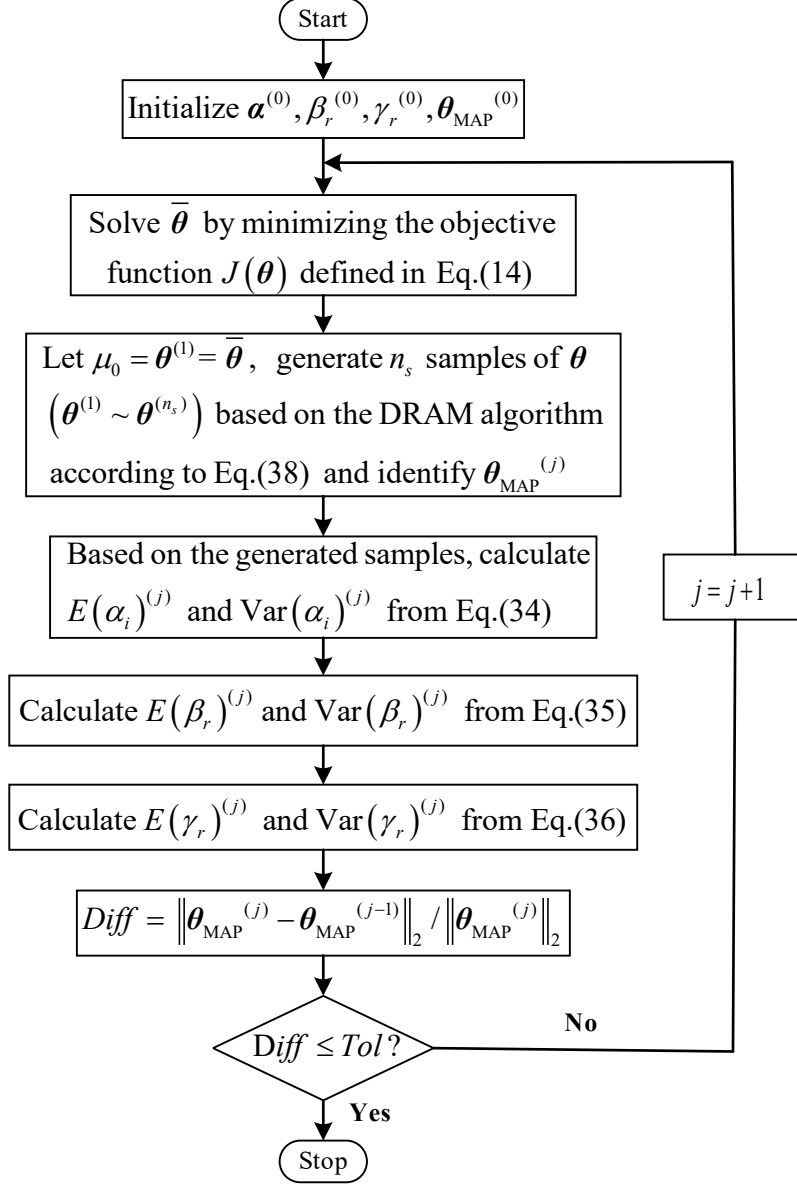


Figure 1 Flowchart of the proposed VBI-DRAM method

6. Experimental Example

6.1 Model description

A laboratory tested two-storey steel frame is utilised to verify the effectiveness of the proposed algorithm. Figure 2 shows the intact structure. The structure is fixed on the strong floor through a steel plate. The entire frame is 1 m high with two equal storeys, and the span is 0.5 m. The cross-section of all components is $50.0 \times 5.0 \text{ mm}^2$. The mass density of the steel material measures $7.92 \times 10^3 \text{ kg/m}^3$, and the Young's modulus is

estimated as $2.0 \times 10^{11} \text{ N/m}^2$.



Figure 2 Experimental frame

A modal test on the intact frame was firstly conducted. The frame was excited using a hammer with a rubber tip. The vibration responses were recorded at 26 locations with equal spacing of 100 mm, as shown in Figure 3. The first eight frequencies and mode shapes were extracted using a rational fraction polynomial method.⁴⁹

Three cuts were then sequentially introduced to the frame. The cuts had the same length of 20 mm and different depths to simulate various damage severities. Specifically, Cut 1 was located at the clamped end with a depth of 10 mm. Cuts 2 and 3 were located at the beam–column joint and the middle of the bottom column with the same depth of 15 mm. Figure 3 shows the configurations and locations of the three cuts.

The structure is modelled using 150 Euler–Bernoulli beam elements with each 20 mm long. Given that the cuts have the same length with each element, the damage severity of each cut defined in Eq. (5) is equal to the reduction in the moment of inertia of the cross-section. Therefore, the SRFs of each damaged element are 40%, 60% and 60%,

respectively, that is, $\theta_1 = -40\%$, $\theta_{126} = -60\%$ and $\theta_{12} = -60\%$, respectively.

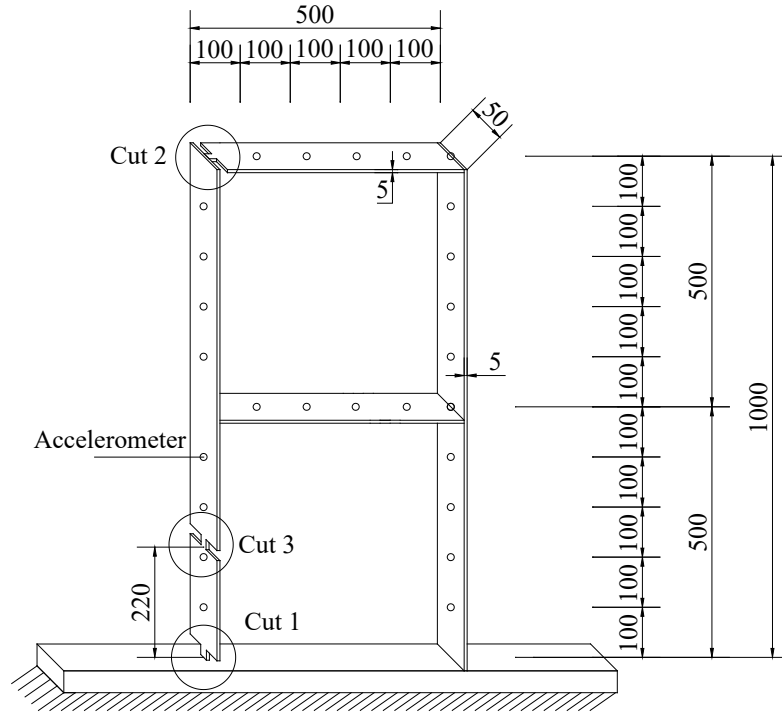


Figure 3 Configuration of the experimental frame and damage locations (unit: mm)

The specific information of three damage scenarios (DSs) is summarized in Table 1. The aforementioned modal test was conducted on each DS. The frequencies and mode shapes of each DS are compared in Table 2. The 6th mode was close to the 7th mode, leading to modal identification errors. These two modes were then removed, and only the first five modes and 8th mode were used for damage identification hereinafter.

Table 1 Damage locations and severities of three DSs

Damage Scenario	Cut No.	Element No.	Cut depth (mm)	Damaged component	SRF (θ)
DS1	Cut 1	1	10	Column	$\theta_1 = -40\%$
DS2	Cut 1	1	10	Column	$\theta_1 = -40\%$
	Cut 2	126	15	Beam	$\theta_{126} = -60\%$
DS3	Cut 1	1	10	Column	$\theta_1 = -40\%$
	Cut 2	126	15	Beam	$\theta_{126} = -60\%$
	Cut 3	12	15	Column	$\theta_{12} = -60\%$

Table 2 Modal data of the frame in undamaged and damaged states (units: Hz)

Mode	Undamaged	DS1		DS2		DS3	
		Freq. (HZ)	MAC	Freq. (HZ)	MAC	Freq. (HZ)	MAC
1	6.27	6.19(-1.39)	0.99	6.17(-1.60)	0.91	6.16(-1.78)	0.96
2	20.64	20.45(-0.92)	0.99	20.16(-2.33)	0.99	20.17(-2.28)	0.87
3	44.35	44.17(-0.40)	0.98	43.89(-1.03)	0.96	43.94(-0.90)	0.93
4	62.63	62.41(-0.36)	0.99	61.69(-1.51)	0.99	61.40(-1.96)	0.98
5	71.29	70.62(-0.93)	0.97	69.98(-1.84)	0.97	69.60(-2.37)	0.95
8	106.52	105.6(-0.90)	0.94	105.1(-1.32)	0.91	104.2(-2.21)	0.88
Average (%)		(-0.82)	0.98	(-1.61)	0.96	(-1.92)	0.93

Note. (1) Values in parentheses are the frequency change ratios (%) between the damaged and undamaged states.

(2) MAC refers to the Modal Assurance Criterion of the mode shapes in the damaged and undamaged states

6.2 Damage identification results

The parameters should be initialised first. As previously mentioned, the VBI does not ensure the global optimum upon convergence. The parameters are recommended to be initialised with different values. Nevertheless, the DRAM algorithm is a relatively global technique that is applicable to nonstandard and nonconvex PDFs, which compensates for the limitation of VBI. Therefore, the θ_{MAP} identified from the samples generated by the DRAM algorithm will be the global maximum theoretically. As previously defined, the parameters reflect the uncertainty level of the selected model. Consequently, these parameters are supposed to converge to the determined values under different initialisations. This will be investigated later. The uncertainty levels of the damage index, frequency and mode shape are initially assumed as 10%, 1% and 5%, respectively, that is, $\alpha_i^{(0)}=1/(10\%)^2=100$ ($i=1, 2, \dots, 150$), $\beta_r^{(0)}=1/(1\%)^2=1 \times 10^4$ ($r=1, 2, \dots, 5, 6$), and $\gamma_r^{(0)}=1/(5\%)^2=400$ ($r=1, 2, \dots, 5, 6$). θ_{MAP} is initialised to $\mathbf{0}$, that is, $\theta_{\text{MAP}}^{(0)} = \mathbf{0}$.

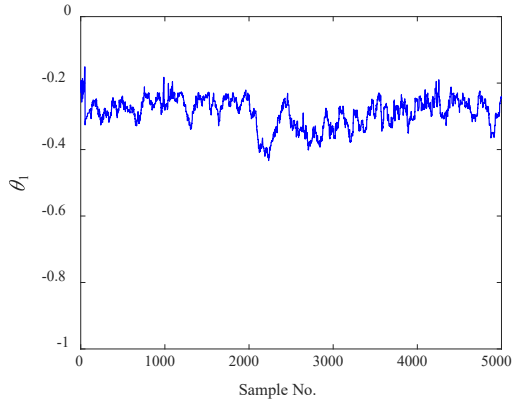
After the initialisation, $\bar{\theta}$ is firstly solved according to Eq.(14). The DRAM algorithm is then carried out to sample θ according to the target PDF Eq. (38). The first sample $\theta^{(1)}$ and mean μ of the proposed PDF are set as $\bar{\theta}$, that is, $\theta^{(1)} = \mu =$

$\bar{\theta}$. The covariance matrix C in Step 1 is assumed as a diagonal matrix with the entry equal to 0.05 and subsequently adjusted according to Step 8. Scale factor ρ is set to 0.01, and $S_d = 2.4^2/d$ (d is the dimension of θ , 150 here). The bound N_t is set to 100. ε is set to 10^{-5} to ensure that the covariance is positive and semidefinite. The number of samples n_s is set to 5000. After obtaining n_s samples of θ , the most probable value θ_{MAP} and expectations $E(\theta_i^2)$, $E\left(\left[\frac{\hat{\lambda}_r - \lambda_r(\theta)}{\hat{\lambda}_r}\right]^2\right)$ and $E\left(\|\hat{\phi}_r - \phi_r(\theta)\|_2^2\right)$ are calculated. Parameters $\{\alpha, \beta, \gamma\}$ are then updated according to Eqs. (34)–(36). The above procedures are repeated until the convergence condition is satisfied ($Tol = 0.02$). The damage index θ and parameters $\{\alpha, \beta, \gamma\}$ are valued as $\theta = \theta_{\text{MAP}}$, $\alpha_i = E(\alpha_i)$, $\beta_r = E(\beta_r)$ and $\gamma_r = E(\gamma_r)$.

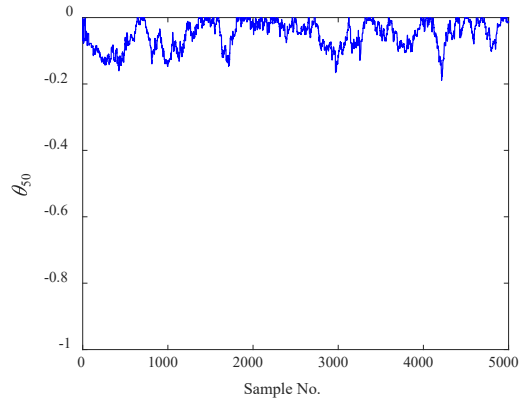
(1) DS1

The actual damage in DS1 is $\theta_1 = -40\%$. In the first iteration, the generated 5000 samples of θ based on the DRAM algorithm and their probability histograms are plotted in Figure 4. For brevity, only the samples of θ_1 and θ_{50} , which correspond to the damaged and undamaged elements, respectively, are presented. Since the mean of the proposed Gaussian PDF and the initial sample are obtained by minimising the objective function Eq.(14), the samples quickly converge to the region nearby the actual damage index. The burn-in period³⁰ in the sampling process is very short, as shown in Figures 4(a) and (b). The probability histograms and fitted PDF curves are plotted in Figures 4(c) and (d), respectively. The posterior PDFs of the damage indices are not standard distributions.

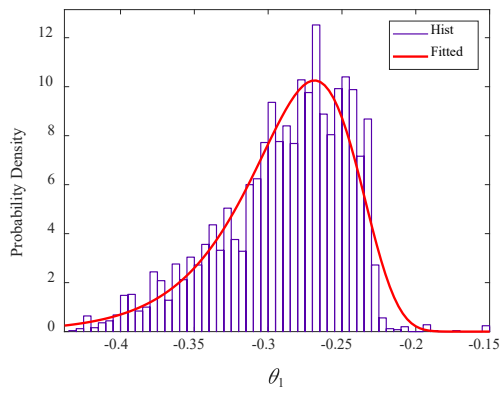
The damage detection results in the first iteration are shown in Figure 5(a). The results show that a number of elements are falsely identified as damaged at the beginning. Convergence is achieved after five iterations, as shown in Figure 5. The actual damaged element No.1 is correctly identified upon convergence. The samples in the final iteration are plotted in Figure 6. Again the posterior PDFs of the damage indices are not standard distributions.



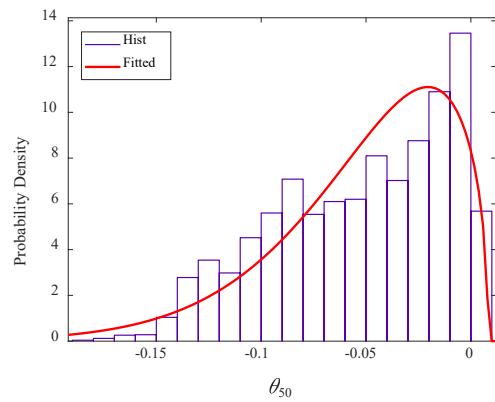
(a) Samples of θ_1



(b) Samples of θ_{50}

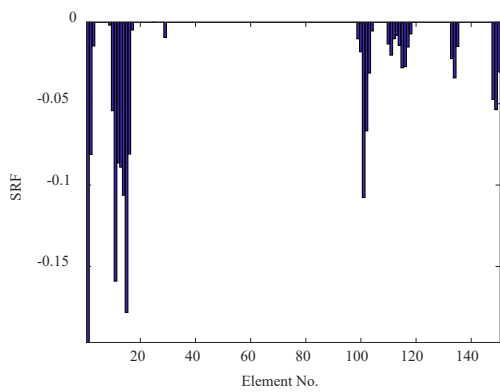


(c) Posterior PDF of θ_1

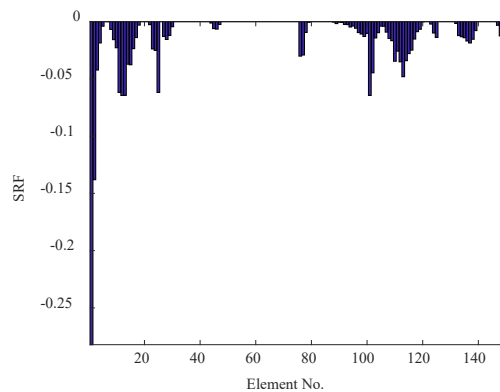


(d) Posterior PDF of θ_{50}

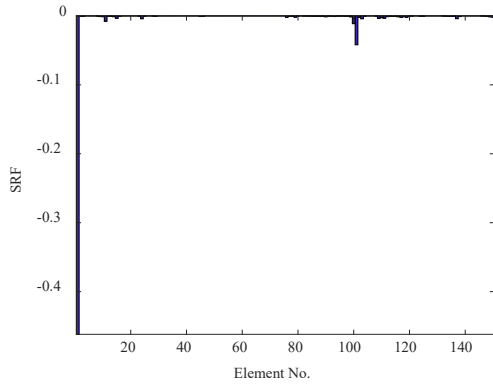
Figure 4 Samples and posterior PDFs in the first iteration (DS1)



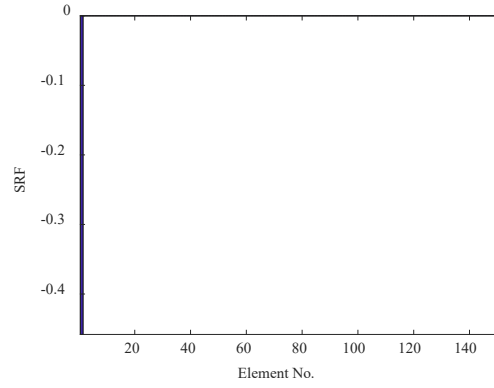
(a) Iteration No.1



(b) Iteration No.2

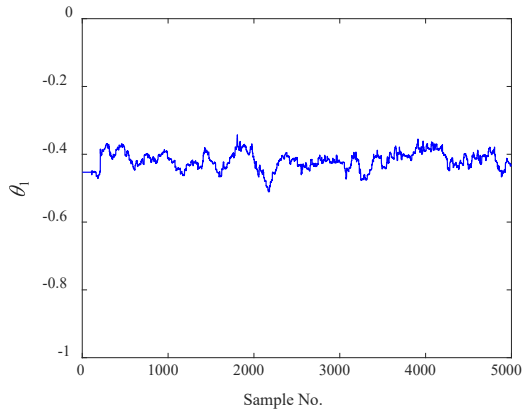


(c) Iteration No.4

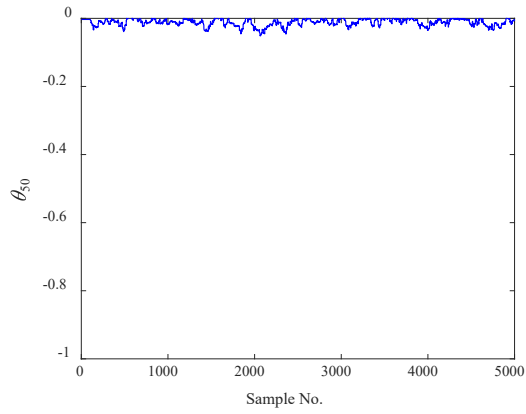


(d) Iteration No.5

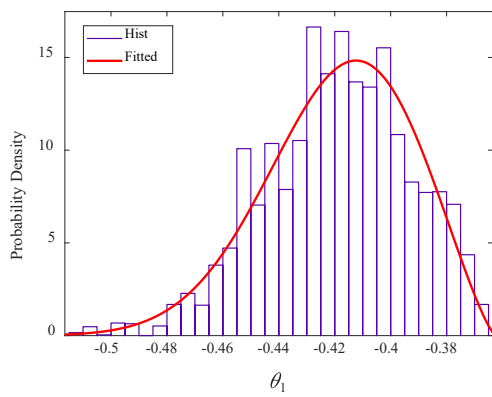
Figure 5 Damage identification results in DS1



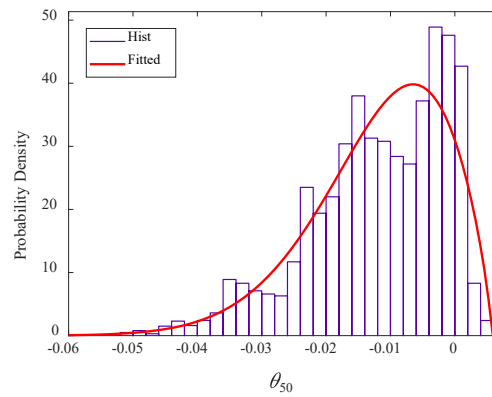
(a) Samples of θ_1



(b) Samples of θ_{50}



(c) Posterior PDF of θ_1



(d) Posterior PDF of θ_{50}

Figure 6 Samples and posterior PDFs in the final iteration (DS1)

(2) DS2

The actual damage in DS2 are $\theta_1 = -40\%$ and $\theta_{126} = -60\%$. The proposed

method is similarly applied to this DS. The samples and PDFs of θ are not shown for brevity. The detection results during the iterations are shown in Figure 7. In the second iteration, element No. 50 is incorrectly identified as damaged, which is located at the top of the column and is adjacent to element No. 126. Upon convergence, this error is eliminated and the two actual damaged elements are correctly identified without false identifications.

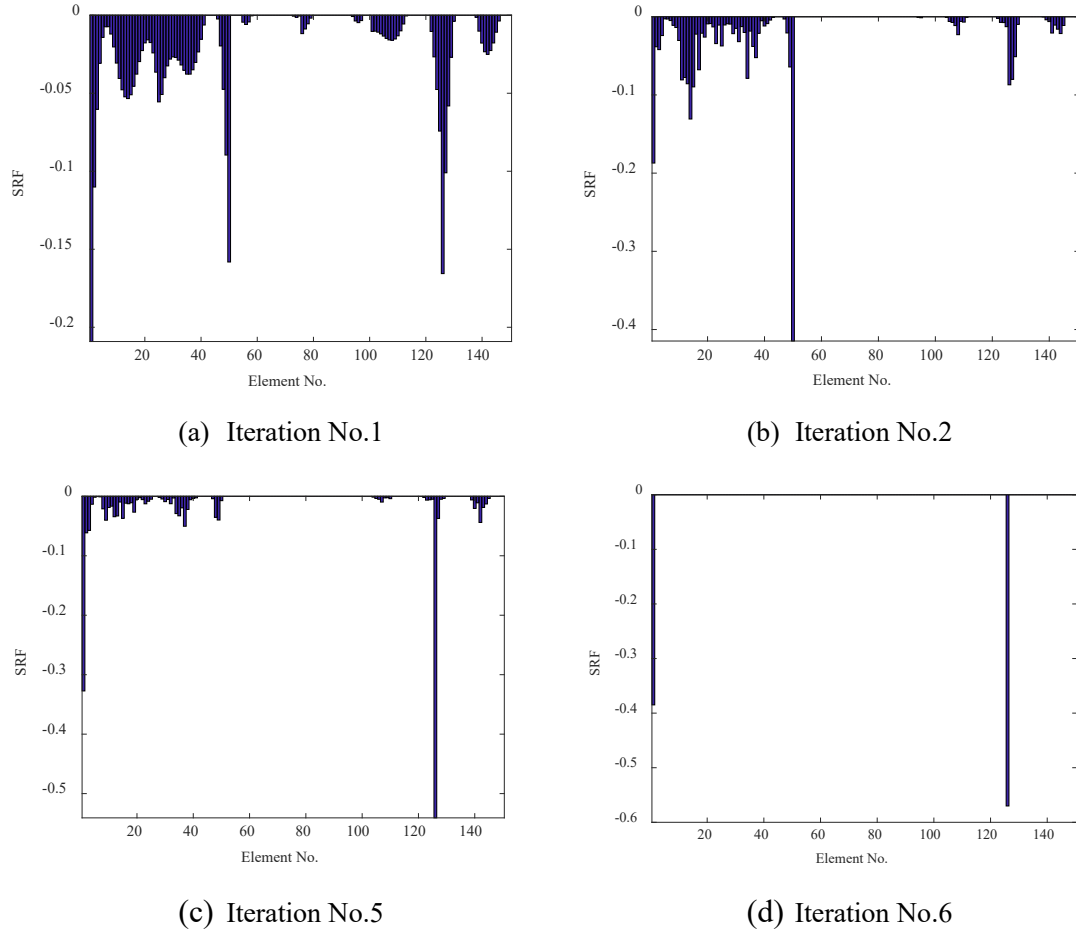
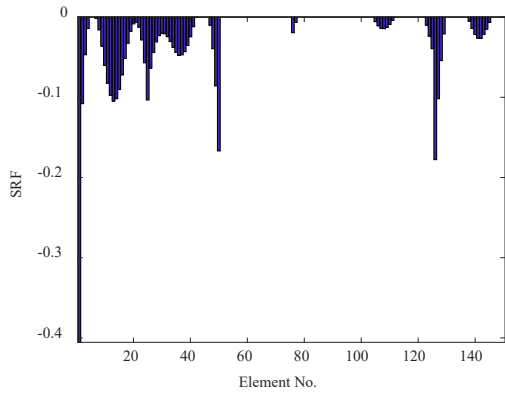


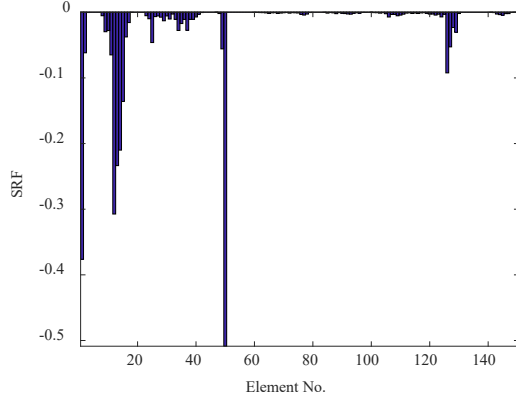
Figure 7 Damage identification results in DS2

(3) DS3

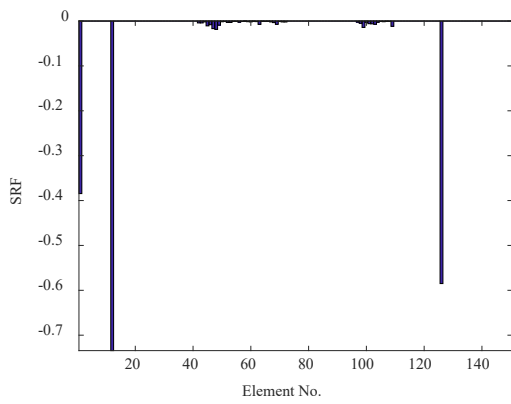
The actual damage in DS3 are $\theta_1 = -40\%$, $\theta_{126} = -60\%$ and $\theta_{12} = -60\%$. The identification results during the iterations are shown in Figure 9. Convergence is achieved after seven iterations. Three damaged elements are accurately identified upon convergence.



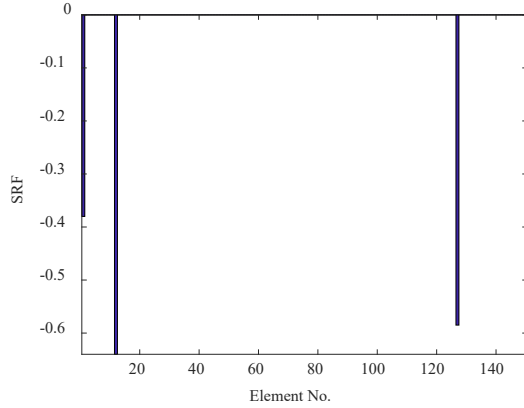
(a) Iteration No.1



(b) Iteration No.2



(c) Iteration No.6



(d) Iteration No.7

Figure 8 Damage identification results in DS3

6.3 Variation of parameters

The parameters also change during the iteration. Figure 9 shows the variations of $\{\alpha, \beta, \gamma\}$ in DS1. In particular, although all α_i ($i = 1, 2, \dots, 150$) have identical initialisation, α_1 converges to a small value close to 1 whereas the remaining α_i ($i=2, 3, \dots, 150$) become significantly large, forcing the corresponding damage indices of undamaged elements to zero in Eq. (14). Consequently, the damage detection results are sparse, which is consistent with the sparsity mechanism of the ARD model. Similar results were obtained by Hou et al.²⁰ The variations of parameters β_r and γ_r in DS1 are presented in Figure 9 (b) and (c). These parameters are different from each other, representing the different uncertainties of each mode.

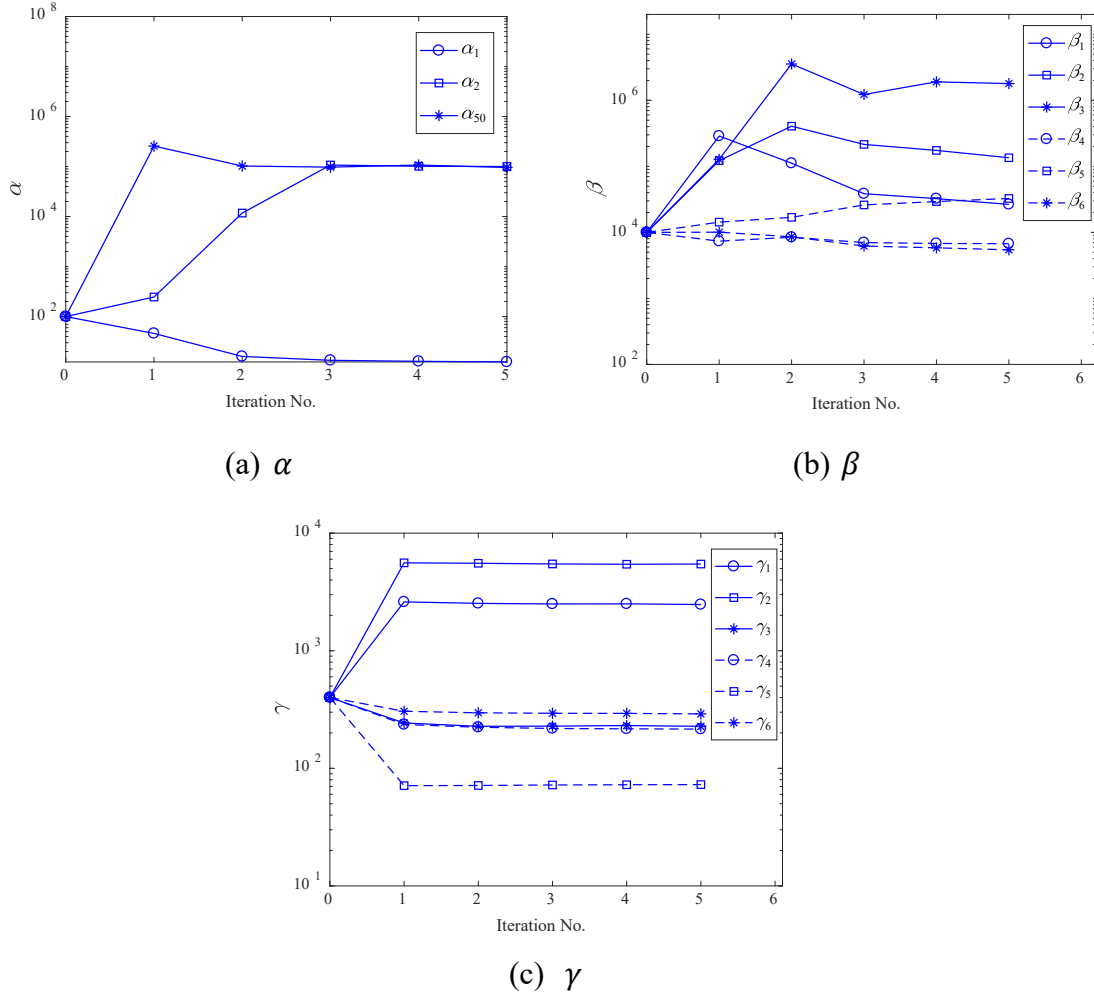


Figure 9 Variations of parameters in DS1 during the iterative process

Two extra groups of values are introduced to the parameters in DS1, that is, $\beta^{(0)}=1/(2\%)^2=2.5\times 10^3$, $\gamma^{(0)}=1/(10\%)^2=100$ and $\beta^{(0)}=1/(0.5\%)^2=4\times 10^4$, $\gamma^{(0)}=1/(2.5\%)^2=1600$, to investigate the effects of different initialisations on the damage detection results using the proposed VBI-DRAM algorithm. The above damage detection process is similarly conducted. Parameters β_1 , β_6 , γ_1 and γ_6 with different initialisations are compared in Figure 10. As it shows, the parameters converge to the identical values in the final iteration step. In particular, $\beta_1=2.8\times 10^4$, $\beta_6=5.2\times 10^3$, $\gamma_1=2.5\times 10^3$ and $\gamma_6=2.9\times 10^2$. Accordingly, the uncertainties of the 1st and 8th eigenvalues are 0.6% and 1.4%, respectively, and those of modal shapes are 2.0% and 5.9%, respectively.

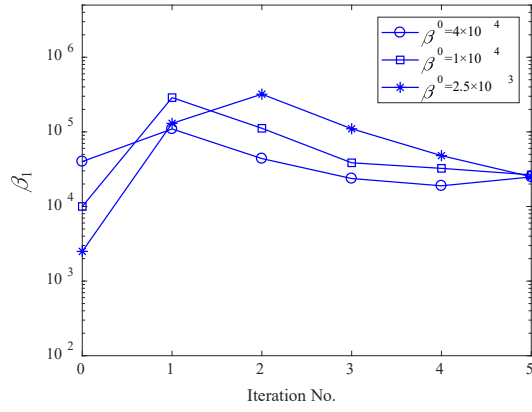
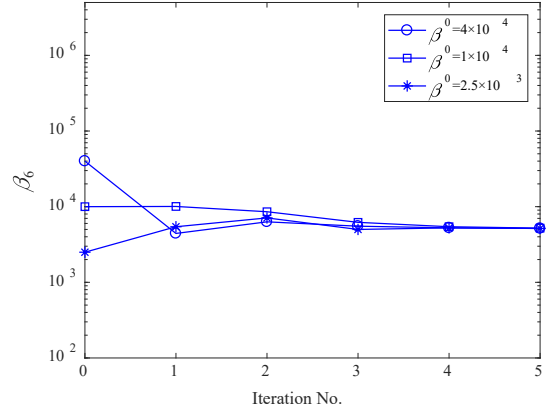
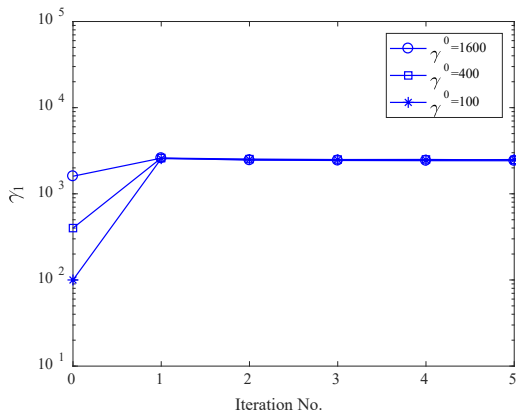
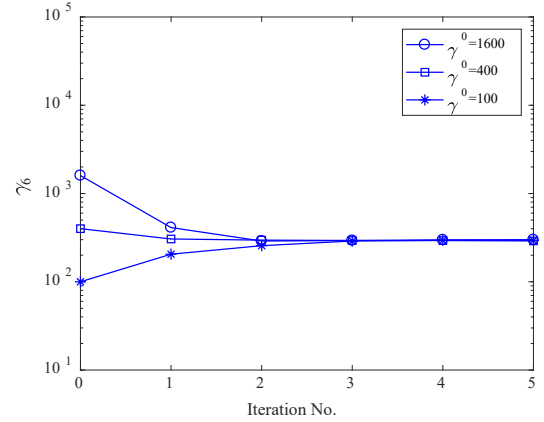
(a) β_1 (b) β_6 (c) γ_1 (d) γ_6

Figure 10 Parameters with different initializations

7. Comparison with the EM method²⁰

A sparse Bayesian learning for damage detection using the expectation-maximization (EM) technique has been developed in Hou et al.²⁰ The present study is an improvement from the theoretical and computational perspectives.

- (1) From the theoretical aspect, the uncertainty of each mode is assumed independently in this study while most other studies treat uncertainties associated with different modes as identical. Also, the posterior uncertainties of parameters $\{\alpha, \beta, \gamma\}$ are taken into consideration in the calculation of θ while Hou et al.,²⁰ did not consider these uncertainties. Finally, the method does not require the posterior PDF following the Gaussian distribution and is thus more widely applicable.

(2) From the computational point of view, the EM technique requires to calculate the Hessian matrix in the posterior sampling or assuming the variance empirically in the likelihood sampling, both are very time-consuming. In the present VBI, the calculation of the Hessian matrix is avoided. The numerical sampling of the damage index θ is directly conducted on the PDF (Eq.(38)), which is proportional to its posterior PDF.

The cantilever beam in Hou et al.²⁰ (Figure 11) is used here for comparing the performance of the present and the EM techniques. The beam is 900 mm long, 50.75 mm wide and 6.0 mm thick with the mass density of $7.67 \times 10^3 \text{ kg/m}^3$. The Young's Modulus of the material is estimated to be $2.0 \times 10^{11} \text{ N/m}$.

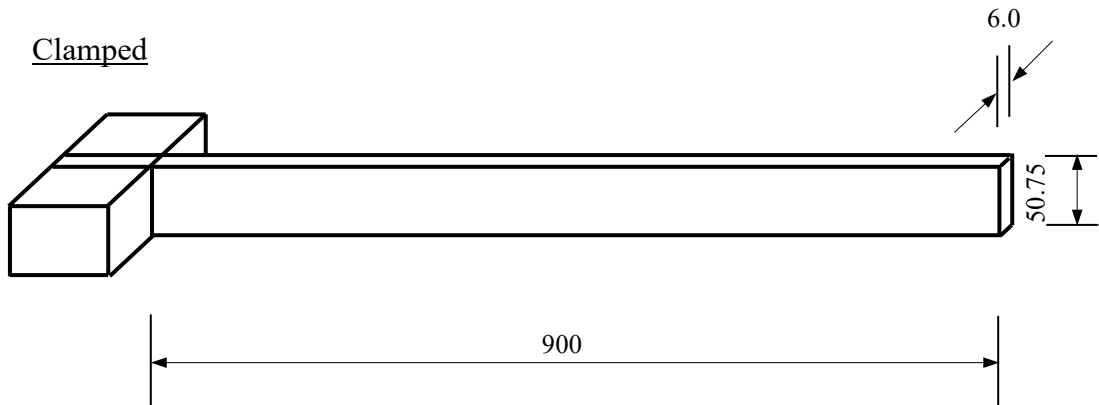


Figure 11 Geometric configuration of the beam structure (unit: mm)

The beam is divided 150 equal Euler-Bernoulli beam elements (i.e. $n = 150$) each having a length of 6 mm. Two cuts are introduced in the clamped end and the middle of the beam with the damage severity of 50%, that is, $\theta_1 = \theta_{75} = -0.5$. The first two frequencies and mode shapes are employed for the model updating and damage detection. The mode parameters in the undamaged and damaged states are listed in Table 3.

Table 3 Modal data of the beam in undamaged and damaged states

Mode	Undamaged	Damaged	
	Freq. (Hz)	Freq. (Hz)	MAC
1	6.02	5.93(-1.50)	1.0000
2	37.75	37.04(-1.88)	0.9998
Average (%)		(-1.69)	0.9999

Note. (1) Values in parentheses are the frequency change ratios (%) between the damaged and undamaged states.
 (2) MAC refers to the Modal Assurance Criterion of the mode shapes in the damaged and undamaged states

The VBI-DRAM method developed in the present study and the EM method are separately employed for the damage detection. The calculations are carried out on a PC with AMD A8-8600P Radeon R6 CPU and 8 GB RAM. The identification results and computational time are compared in Table 4. As it shows, the damage detection results using both techniques are accurate, while the computational time using the present VBI-DRAM method is only 7% of that using the EM technique. Consequently, the VBI-DRAM is much more efficient than the other.

Table 4 Damage detection results using EM and VBI-DRAM method

Technique	Result	Time
EM	$\theta_1 = -0.52$	147'36"
(Posterior sampling)	$\theta_{45} = -0.49$	
VBI-DRAM	$\theta_1 = -0.52$ $\theta_{45} = -0.51$	11'19"

8. Conclusions

This study proposes a sparse Bayesian model for structural damage detection based on the VBI and DRAM algorithms. By combining the two techniques, the individual posterior PDF of the damage index and parameters are derived and a full Bayesian treatment of all posterior uncertainties is conducted. The damage index and

parameters are iteratively solved. The proposed method is applicable to standard and nonstandard probability distributions. A laboratory tested frame is utilised to verify its effectiveness. The results indicate that the damage location and severity can be accurately detected. The uncertainty of each mode is different, verifying the rationality of the independent evaluation of each mode in this study. A comparative study demonstrates that it is computationally efficient than the EM technique. The proposed method has the advantages of high accuracy and wide applicability for structural damage detection.

Acknowledgements

This study was supported by the PolyU Research Grant (Project No. 1-ZVP2) and the National Natural Science Foundation of China (Project No. 51678364).

References

1. Zhang J, Xu YL, Xia Y, et al. A new statistical moment-based structural damage detection method. *Structural Engineering and Mechanics* 2008; 30: 445–466.
2. Simoen E, De Roeck G and Lombaert G. Dealing with uncertainty in model updating for damage assessment: A review. *Mechanical Systems and Signal Processing* 2015; 56–57: 123–149.
3. Xia Y and Hao H. Statistical damage identification of structures with frequency changes. *Journal of Sounds and Vibration* 2003; 263: 853–870.
4. Doebling SW, Farrar CR, Prime MB, et al. Damage identification and health monitoring of structural and mechanical systems from changes in their vibration characteristics: a literature review. Los Alamos National Laboratory Report, 1996.
5. Sohn H, Farrar CR, Hemez FM, et al. A review of structural health monitoring literature: 1996–2001, Los Alamos National Laboratory Report, 2003.
6. Hua XG, Ni YQ, Chen ZQ, et al. An improved perturbation method for stochastic finite element model updating. *International Journal for Numerical Methods in Engineering* 2008; 73: 1845–1864.
7. Yeo I, Shin S, Lee HS, et al. Statistical damage assessment of framed structures from static responses. *Journal of Engineering Mechanics, ASCE* 2000; 126: 414–421.
8. Gul M and Catbas FN. Statistical pattern recognition for structural health monitoring using time series modeling: theory and experimental verifications, *Mechanical Systems and Signal Processing* 2009; 23: 2192–2204.
9. Beck JL and Katafygiotis LS. Updating models and their uncertainties. I: Bayesian statistical framework, *Journal of Engineering Mechanics, ASCE* 1998; 124: 455–461.
10. Ching J and Beck JL. Bayesian analysis of the Phase II IASC-ASCE structural health monitoring experimental benchmark data. *Journal of Engineering Mechanics, ASCE* 2004; 130: 1233–1244.
11. Zhu YC and Au SK. Bayesian operational modal analysis with asynchronous data, part I: Most probable value. *Mechanical Systems and Signal Processing* 2018; 98: 652–666.
12. Yan WJ and Katafygiotis LS. An analytical investigation into the propagation properties of uncertainty in a two-stage fast Bayesian spectral density approach for ambient modal analysis. *Mechanical Systems and Signal Processing* 2019; 118: 503–533.
13. Huang Y, Shao CS, Wu BA, et al. State-of-the-art review on Bayesian inference in structural system identification and damage assessment. *Advances in*

- Structural Engineering* 2019; 22: 1329–1351.
14. Tipping ME. Sparse Bayesian learning and the relevance vector machine, *Journal of Machine Learning Research* 2001; 1: 211–244.
 15. Malioutov D, Cetin M and Willsky AS. A sparse signal reconstruction perspective for source localization with sensor arrays. *IEEE Transactions on Signal Processing* 2005; 53: 3010–3022.
 16. Fang J, Shen YN, Li FW, et al. Support knowledge-aided sparse Bayesian learning for compressed sensing. *IEEE International Conference on Acoustics* 2015, 3786–3790.
 17. Huang Y and Beck JL. Hierarchical sparse Bayesian learning for structural health monitoring with incomplete modal data. *International Journal for Uncertainty Quantification* 2015; 5: 139–169.
 18. Huang Y, Beck JL and Li H. Hierarchical sparse Bayesian learning for structural damage detection: theory, computation and application. *Structural Safety* 2017; 64: 37–53.
 19. Huang Y, Beck JL and Li H. Bayesian system identification based on hierarchical sparse Bayesian learning and Gibbs sampling with application to structural damage assessment. *Computer Methods in Applied Mechanics and Engineering* 2017; 318: 382–411.
 20. Hou RR, Xia Y, Zhou XQ, et al. Sparse Bayesian learning for structural damage detection using expectation-maximization technique. *Structural Control and Health Monitoring* 2019; 26.
 21. Wang XY, Hou RR, Xia Y, et al. Laplace approximation in sparse Bayesian learning for structural damage detection. *Mechanical Systems and Signal Processing*, under review.
 22. Smith AFM and Roberts GO. Bayesian computation via the Gibbs sampler and related Markov-chain Monte-Carlo methods, *Journal of the Royal Statistical Society Series B-Methodological* 1993; 55: 3–23.
 23. Beck JL. Bayesian system identification based on probability logic. *Structural Control and Health Monitoring* 2010; 17: 825–847.
 24. Beal MJ. Variational algorithms for approximate Bayesian inference. PhD thesis, University of London, 2003.
 25. Bishop CM. Pattern recognition and machine learning. Berlin: Springer, 2006.
 26. Parisi G. Statistical field theory. Addison-Wesley, 1988.
 27. Baldacchino T, Cross EJ, Worden K, et al. Variational Bayesian mixture of experts models and sensitivity analysis for nonlinear dynamical systems. *Mechanical Systems and Signal Processing* 2016; 66–67: 178–200.

28. Jacobs WR, Baldacchino T, Dodd T, et al. Sparse Bayesian nonlinear system identification using variational inference. *IEEE Transactions on Automatic Control* 2018; 63: 4172–4187.
29. Blei DM, Kucukelbir A and McAuliffe JD. Variational Inference: a review for statisticians. *Journal of the American Statistical Association* 2017; 112: 859–877.
30. Andrieu C, de Freitas N, Doucet A, et al. An introduction to MCMC for machine learning. *Machine Learning* 2003; 50: 5–43.
31. Chib S and Greenberg E. Understanding the Metropolis-Hastings Algorithm. *American Statistician* 1995; 49: 327–335.
32. Arminger G. A Bayesian approach to nonlinear latent variable models using the Gibbs sampler and the Metropolis-Hastings algorithm. *Psychometrika* 1998; 63: 271-300.
33. Au SK and Beck JL. Estimation of small failure probabilities in high dimensions by subset simulation. *Probabilistic Engineering Mechanics* 2001; 16: 263–277.
34. Yang JH and Lam HF. An efficient adaptive sequential Monte Carlo method for Bayesian model updating and damage detection. *Structural Control and Health Monitoring* 2018; 25.
35. Ching JY and Chen YC. Transitional Markov chain Monte Carlo method for Bayesian model updating, model class selection, and model averaging. *Journal of Engineering Mechanics* 2007; 133: 816–832.
36. Haario H, Saksman E and Tamminen J. Adaptive proposal distribution for random walk Metropolis algorithm. *Computational Statistics* 1999; 14: 375–395.
37. Haario H, Saksman E and Tamminen J. An adaptive Metropolis algorithm, *Bernoulli* 2001; 7: 223–242.
38. Tierney L and Mira A. Some adaptive Monte Carlo methods for Bayesian inference. *Statistics in Medicine* 1999; 18: 2507–2515.
39. Green PJ and Mira A. Delayed rejection in reversible jump Metropolis-Hastings. *Biometrika* 2001; 88: 1035–1053.
40. Mira A. On Metropolis-Hastings algorithms with delayed rejection. *Metron* 2001; 59: 231–241.
41. Haario H, Laine M, Mira A, et al. DRAM: Efficient adaptive MCMC. *Statistics and Computing* 2006; 16: 339–354.
42. Zuev KM and Katafygiotis LS. Modified Metropolis-Hastings algorithm with delayed rejection. *Probabilistic Engineering Mechanics* 2011; 26: 405–412.
43. Zhang J, Wan CF and Sato T. Advanced Markov chain Monte Carlo approach for finite element calibration under uncertainty. *Computer-Aided Civil and*

Infrastructure Engineering 2013; 28: 522–530.

44. Wan HP and Ren WX. Stochastic model updating utilizing Bayesian approach and Gaussian process model. *Mechanical Systems and Signal Processing* 2016; 70–71: 245–268.
45. Zhou XQ, Xia Y and Weng S. l_1 regularization approach to structural damage detection using frequency data. *Structural Health Monitoring* 2015; 14: 571–582.
46. Hou RR, Xia Y and Zhou XQ. Structural damage detection based on l_1 regularization using natural frequencies and mode shapes. *Structural Control and Health Monitoring* 2018; 25.
47. Chen ZP, Pan CD and Yu L. Structural damage detection via adaptive dictionary learning and sparse representation of measured acceleration responses. *Measurement* 2018; 128: 377–387.
48. Wang L and Lu ZR. Sensitivity-free damage identification based on incomplete modal data, sparse regularization and alternating minimization approach. *Mechanical Systems and Signal Processing* 2019; 120: 43–68.
49. Formenti D and Richardson M. Parameter estimation from frequency response measurements using rational fraction polynomials (twenty years of progress). *Proceeding of International Modal Analysis Conference* 2002; 4753: 373–382.